DOI: 10.1002/chem.200701988

Mesoporous Silicas by Self-Assembly of Lipid Molecules: Ribbon, Hollow Sphere, and Chiral Materials

Haiying Jin,[a] Huibin Qiu,[a] Yasuhiro Sakamoto,[b] Peng Shu,[a] Osamu Terasaki,[b] and Shunai Che*[a]

Abstract: Using lipids (*N*-acyl amino acids) and 3-aminopropyltriethoxysilane as structure- and co-structure-directing agents, mesoporous silicas with four different morphologies, that is, helical ribbon (HR), hollow sphere, circular disk, and helical hexagonal rod, were synthesized just by changing the synthesis temperature from 0 °C to 10, 15, or 20 °C. The structures were studied by electron microscopy. It was found that 1) the structures have double-layer disordered mesopores in the HR, radially oriented mesopores in the hollow sphere, and highly ordered straight and chiral 2D-hexagonal mesopores in the disklike structure and helical rod, respectively; 2) these four types of mesoporous silica were transformed from the flat bilayered lipid ribbon with a chain-interdigitated layer phase through a solid–solid transformation for HR formation and a dissolving procedure transformation for the synthesis of the hollow sphere, circular disk, and twisted morphologies; 3) the mesoporous silica helical ribbon was exclusively right-handed and the 2D-hexagonal chiral mesoporous silica was excessively left-handed when the L-form *N*-acyl amino acid was used as the lipid template; 4) the HR was formed only by the chiral lipid molecules, whereas the 2D-hexagonal chiral mesoporous silicas were formed by chiral, achiral, and racemic lipids. Our findings give important information for the understanding of the formation of chiral materials at the molecular level and will facilitate a more efficient and systematic approach to the generation of rationalized chiral libraries.

Keywords: chirality · helical structures · mesoporous materials · self-assembly · silica

Introduction

It is well known that nature uses self-assembly to construct microstructures for the functioning of living organisms. Living systems are constructed through the hierarchical assembly of these microstructures on many different size scales. It is essential to mimic biomolecular self-assembly techniques to design, engineer, and fabricate inorganic nano- and microstructures for the development of advanced materials, such as sensors, catalysts, and separation media.[1]

Carbohydrate amphiphiles and phospholipids are basic building blocks of biomembranes in living systems. By the same fundamental principles, in aqueous media, the lipid molecules self-assemble into diverse microstructured aggregate morphologies, which depend on both the molecular shape of the molecules and on solution conditions, such as lipid concentration, pH value, and temperature.[2] Among these morphologies, electrolyte vesicles,[3] ultrathin membranes,[4] nanotubes,[5] helical ribbons,[6] helical tubes,[7] and others[8] have been utilized as templates to create nanosized and microstructured inorganic materials. More advanced materials, techniques, and fabrication mechanisms must be developed to produce these self-assembled nano- and microstructured inorganic materials.

Recently, we discovered a templating route for preparing well-ordered mesoporous silica based on the self-assembly of anionic surfactants and inorganic precursors in the presence of an aminosilane or quaternary aminosilane as a co-structure-directing agent (CSDA);[9] this method opened up new possibilities for the synthesis of mesoporous materials

[a] H. Jin, H. Qiu, P. Shu, Prof. S. Che
School of Chemistry and Chemical Technology
State Key Laboratory of Composite Materials
Shanghai Jiao Tong University
800 Dongchuan Road, Shanghai, 200240 (China)
Fax: (+86) 21-5474-5365
E-mail: chesa@sjtu.edu.cn

[b] Dr. Y. Sakamoto, Prof. O. Terasaki
Structural Chemistry and Berzelii centre EXSELENT on Porous Materials
Arrhenius Laboratory, Stockholm University
10691 Stockholm (Sweden)

Supporting information for this article is available on the WWW under http://www.chemeurj.org/ or from the author.

 © 2008 Wiley-VCH Verlag GmbH & Co. KGaA, Weinheim

by using anionic amphiphilic lipid molecules. In our previous work, we synthesized 2D-hexagonally ordered chiral mesoporous silica by using *N*-miristoyl-L-alanine sodium salt (C_{14}-L-AlaS) partially neutralized in HCl (HCl/C_{14}-L-AlaS = 0.08–0.10) at a reaction temperature of 80 °C, with an aminosilane or a quaternized aminosilane as a CSDA.[10]

Here, we approached the synthesis of a mesoporous silica helical ribbon (HR) by controlling the assembly behavior of an *N*-acyl amino acid (*N*-AAA) upon variation of the synthesis temperature. It is well known that many amphiphilic molecules spontaneously self-assemble to produce vesicles, ribbons, and tubes with bi- or multilayerd structures upon cooling, as reported by Schnur, by Shimizu et al., and by Clark and co-workers.[1,2,11] Therefore, our approach was based on controlling the self-assembled structures formed from partially neutralized carboxylate surfactants upon cooling of the synthesis system from a higher temperature. When the partially neutralized anionic *N*-AAA, CSDA (3-aminopropyltriethoxysilane, APES), and silica source (tetraethoxylsilane, TEOS) are mixed, the mesoporous silica can be formed through electrostatic interactions between the head group of the surfactant and the amino group of APES and through cocondensation of the silane side of APES and TEOS.[10]

The temperature of the reaction system is an important factor in determining the assembly structure because both the thermodynamics of the lipid molecules and the kinetics of the hydrolysis of TEOS followed by condensation/polymerization are strongly dependent on temperature. Here, HRs with bilayer structures have been formed at lower temperatures and other highly ordered mesoporous silicas have been formed at higher temperatures. To observe the structural evolution of the mesophases during synthesis, scanning electron microscopy (SEM) images, high-resolution transmission electron microscopy (HRTEM) images, and X-ray diffraction (XRD) patterns of the products were obtained as a function of the reaction time. It was speculated that reassembly of the flat lipid ribbon, achieved by coupling of the silica precursors, may be the origin of the mesoporous silica HR and other mesoporous silicas. Antipodal L and D forms along with racemic and achiral lipid molecules have been used for evaluating the dependence of different mesostructure formations on the molecular chirality.

Results and Discussion

Temperature dependence of the formation of different mesoporous silicas: Among the *N*-AAAs, C_{14}-L-AlaS has been chosen as an example here to show the experimental results in detail. Different mesoporous silicas were synthesized within a temperature range of 0–20 °C over 1 day (see the Experimental Section for details). SEM images, HRTEM images, XRD patterns, and nitrogen adsorption–desorption results for samples synthesized at 0, 10, 15, and 20 °C are shown in Figures 1–4, respectively. All of the samples were composed of particles that were uniform in shape: the particles have well-defined external morphologies that depend on the synthesis temperature.

The sample synthesized at 0 °C (Figure 1A) consisted exclusively of HR structures with a uniform width of 200–250 nm and thickness of 30–35 nm, which form a tubular

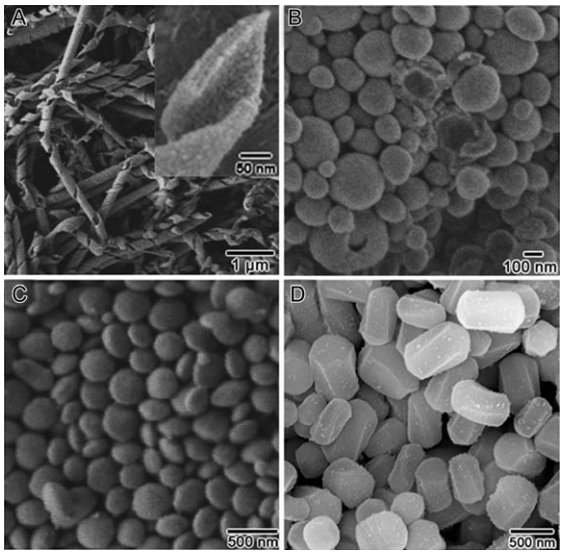

Figure 1. SEM images of extracted mesoporous silicas synthesized at different temperatures at 0 °C (A), 10 °C (B), 15 °C (C), and 20 °C (D). The synthesis molar composition was C_{14}-L-AlaS:APES:TEOS:HCl:H_2O 1:1:7:0.1:1780.

structure with a constant pitch length of 500–700 nm and an outer diameter of 150–200 nm. This HR microstructure is analogous to one found in folded proteins (protein α/β helix). From the magnified SEM image (inset of Figure 1A) of the cross-section of HR, it can be observed that two parallel porous systems exist in it without penetrating through the wall; this has also been observed from TEM images (see below). A few rolled-up sheets were also observed in this sample. As far as can be observed, all of the tubular ribbons show a right-handed (*P*) helical motif, regardless of whether they are HRs or rolled-up sheets. The existence of mesopores within the tubular-ribbon wall was confirmed by the higher magnification HRTEM images (Figure 2A) and the nitrogen adsorption–desorption isotherms (Figure 4A). As shown in Figure 2A, the mesoporous silica HR consists of adhered double layers with the same thickness of about 15 nm and possesses disordered mesoporous channels perpendicular to the central axis of the tube and distributed uniformly in the wall. No resolved peaks were observed from the XRD patterns (Figure 3A), largely because of the presence of the disordered pores in the thin walls.

The SEM image shows that irregular spherical particles were formed at 10 °C, as shown in Figure 1B. These spheres are small (100–400 nm) in diameter and have a broad size distribution. From the cracked spheres, the hollow centers can be observed clearly. The HRTEM image (Figure 2B) shows that these spheres possess hollow centers with an

 © 2008 Wiley-VCH Verlag GmbH & Co. KGaA, Weinheim

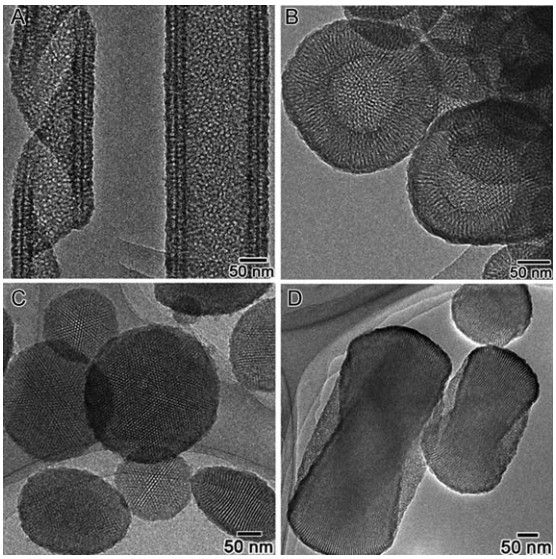

Figure 2. Respective TEM images of the samples shown in Figure 1.

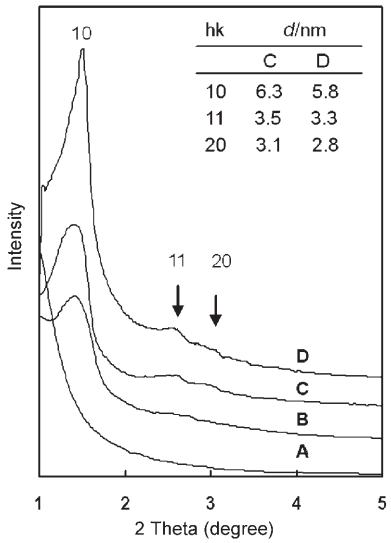

Figure 3. XRD patterns of the samples shown in Figure 1.

inner diameter ranging from 50 to 150 nm and with mesoporous architecture in the walls. The wall thicknesses of the hollow spheres are in the range of 25–60 nm, which is much thicker than the HR walls. It was found that the disordered channels penetrate the walls from the inside to the outside. The XRD pattern (Figure 3B) of this sample shows only one broad peak in the 2θ range of 1–2°, which indicates the existence of the disordered pore system.

The samples synthesized at 15 °C very clearly consisted of exclusively disklike crystals that were spindly from the side view, with diameters of 150–300 nm and heights of 100–150 nm (Figure 1C and Figure 2C). The HRTEM image shows a characteristic image contrast that is similar to that of a 2D-hexagonal structure. The particles images with a side view of the disk (bottom-right crystal) show that the pores seem not to be straight at the edge, and some of the crystals also show unusual image contrast in the top view, as seen in the top-left crystal. From these results, it is estimated that the disklike crystals have a 2D-hexagonal structure, which is consistent with the XRD pattern. However, further discussion is needed to explain the typical image contrast observed in the HRTEM images. The XRD patterns (Figure 3C) of these extracted chiral mesoporous silicas revealed three well-resolved peaks in the range of $2\theta = 1.5$–6°, which were indexed as the 10, 11, and 20 reflections based on the 2D-hexagonal *p6mm* structure (which was also confirmed by TEM observation), with similar values of $a = 6.5$–6.7 nm.

Chiral mesoporous silica (CMS) was formed when the synthesis temperature was further increased to 20 °C (Figure 1D, Figure 2D, and Figure 3D), as reported in our previous work.[12] This material has twisted hexagonal rodlike morphology, with diameters of 300–500 nm and lengths of 400–800 nm. The XRD pattern and HRTEM images confirm the presence of hexagonally ordered chiral channels of 6.0 nm in diameter winding around the central axis of the rods. The handedness of this chiral mesoporous hexagonal rod was estimated by counting the characteristic morphologies from 500 randomly chosen crystals in the SEM images, and left-/right-handed ratios proved to be 7.5/2.5, that is, the left-handed morphology is in excess.

The mesoporous silica HRs synthesized at 0 °C show capillary-condensation steps in the relative pressure range of 0.4–0.7 (Figure 4A); this corresponds to adsorption in uniform mesopores of about 3.6 nm. The BET surface area and pore volume are 349 $m^2 g^{-1}$ and 600 $mm^3 g^{-1}$, respectively. Nitrogen adsorption–desorption isotherms of the hollow sphere, disklike, and CMS structures (Figure 4B, C, and D, respectively) show type IV features with capillary-condensation steps with significant hysteresis loops at a relative pressure of about 0.4, thereby indicating the existence of uniform mesopores. These three types of materials possess simi-

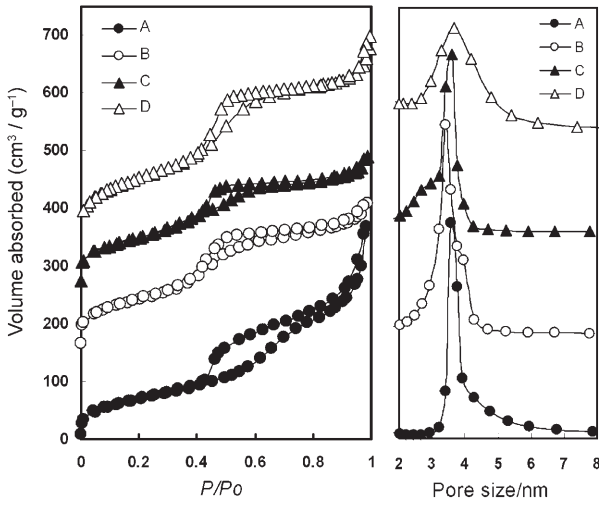

Figure 4. Nitrogen adsorption–desorption isotherms and pore-size distributions of samples shown in Figure 1.

 © 2008 Wiley-VCH Verlag GmbH & Co. KGaA, Weinheim

lar pore diameters of about 3.6 nm, and the BET surface areas and pore volumes are in the range of 300–400 $m^2 g^{-1}$ and 300–400 $mm^3 g^{-1}$, respectively.

Structural evolution of the mesophases during the synthesis: To investigate the structural evolution of the mesophases during synthesis, SEM images (Figure 5) and XRD patterns (Figure 6) of the products were observed as a function of the reaction time. First, in order to find evidence for the surfactant-derived lipid-templating effect, the organic lipid was prepared and its morphology was characterized. The gel formed upon addition of HCl at the first stage was freeze dried before APES and TEOS were added, and the water was then removed by evacuation. Mesophases originating from the same initial mixture were sampled at different reaction times over 2 h. Accumulated flat tapes with a length of several microns or more were observed from the SEM images of the freeze-dried lipid organogel (Figure 5). XRD patterns taken at low angles enabled us to determine the mesostructure of the lipid. The diffraction pattern of the freeze-dried lipid organogel (Figure 6) shows Bragg peaks for typical lamellar organization. The three well-resolved sharp peaks, indexed as the 1, 2, and 3 reflections in the region of $2\theta = 1.0$–$9.0°$ with a d spacing of about 2.8 nm,

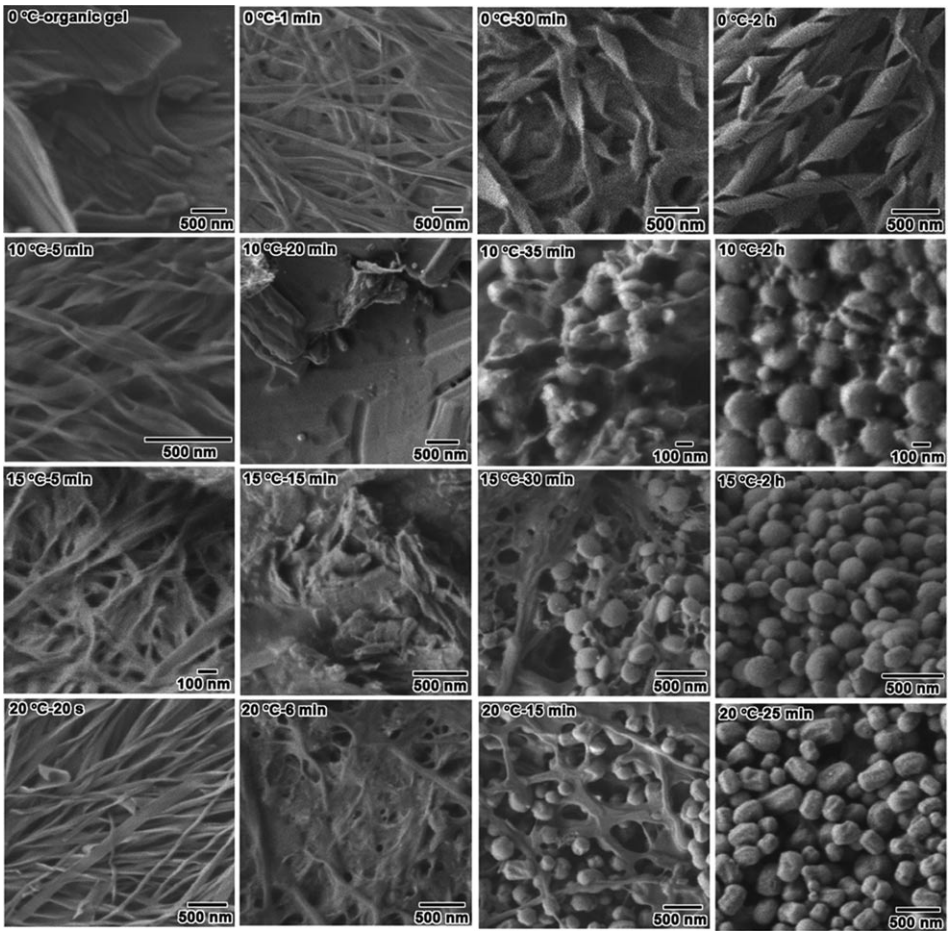

Figure 5. SEM images of the freeze-dried lipid organic gel and the as-synthesized products sampled at different reaction times and different reaction temperatures.

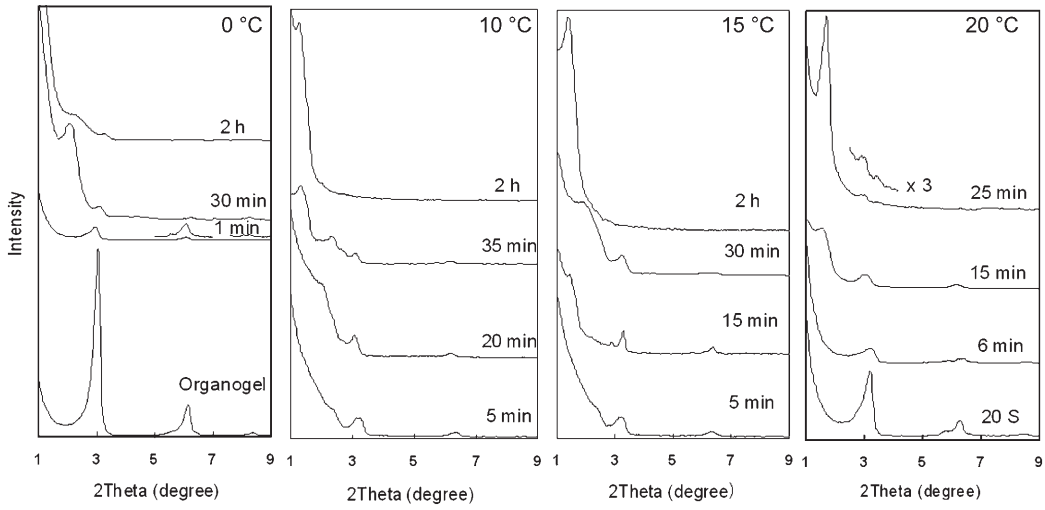

Figure 6. XRD patterns of samples shown in Figure 5.

© 2008 Wiley-VCH Verlag GmbH & Co. KGaA, Weinheim

suggest an interdigitated layer structure, since the extended molecular length of C_{14}-L-AlaS can be evaluated as about 2.5 nm. The interdigitation means that hydrophilic carboxyl head groups are present on both the inner and outer surfaces of the organic tube in water.[6c]

Figure 5 (0 °C) shows SEM images of the freeze-dried lipid organogel and the samples synthesized at 0 °C with different reaction times. After addition of APES and TEOS into the lipid gel with flat-tape morphology, it was found that the morphology changed from flat tapes (1 min) to loosely coiled HRs (30 min) with pitch lengths of 750–900 nm and finally to tightly coiled HRs with pitch lengths of 500–700 nm or paper-roll-like tubules (2 h). The width and thickness of the ribbons increased gradually as the reaction proceeded. The width of the flat ribbons increased from 100–160 nm to 150–200 nm for the loosely coiled ribbons and finally to 200–250 nm for the tightly coiled ribbons; the thickness increased from 6–7 nm to 30–35 nm. These results indicate that the formation process of helical mesoporous silica tubes involves several metastable intermediate structures; this supports the view that helical mesoporous silica is formed by an anisotropic tape-to-helicity transformation with simultaneous shortening of the helical pitch of the ribbon and widening of the tape. It is particularly noteworthy that all of the HRs are enantiopurely right-handed.

The diffraction pattern of the product sampled at 1 min shows three well-resolved but lower intensity peaks (compared to the results for the lipid organogel), indexed as the 1, 2, and 3 reflections, in the region of $2\theta = 1.0$–$9.0°$ with a d spacing of 2.9 nm; these results indicate a lamellar structure similar to that of the freeze-dried lipid organogel. After 30 min of reaction time, the XRD peaks indexed as lamellar structure decreased and actually disappeared after 2 h. The peak at $2\theta = 2.1°$, due to the disordered mesopores with a d spacing of 4.2 nm, began to grow at the expense of the lamellar peaks. The materials synthesized for 30 min still showed many sharp peaks in the higher 2θ range of 10–40°, which are characteristic of the surfactant (see Figure S1 in the Supporting Information), but when the synthesis was continued to 2 h, all of the peaks disappeared. These results indicate that the state of the lipid amphiphilic molecules changed from the bulk to a uniformly dispersed form in the mesoporous silica as the reaction proceeded.

The formation process of the helical mesoporous silica ribbon is illustrated in Figure 7. First, upon a decrease in the temperature to 0 °C, partially neutralized chiral amphiphilic carboxylate molecules self-assemble into flat tapes with a bilayer structure, through the hydrophobic interaction of the hydrocarbon chains, in which the chiral molecules pack parallel to their nearest neighbors at a zero twist angle with respect to their nearest neighbors (Figure 7a). Hydrogen bonding between the amide groups strengthens such bilayer arrangements, and the chirality of asymmetric carbon atoms demands a helical structure of bilayer strands or coiled ribbons.[13] With the addition of APES and TEOS, the carboxylic acid group will be negatively charged by the amino group of APES through a neutralization reaction. This will increase the charge density of the micelle surface, which consequently increases the electrostatic repulsion between the charged-surfactant head groups and will thus increase in the effective head-group area of the surfactant. At the same time, this will create an arrangement of chiral molecules tilted with respect to the local layer, due to gauche geometry caused by the interaction between the amino groups and the C=O moieties, and the favored twist from neighbor to neighbor leads to the whole ribbon coiling into a tube.[14] Simultaneously, APES and TEOS can easily penetrate into the ribbon from its surface and convert the lipid wall into a mesoporous one through reassembly. The lipid molecules, APES, and TEOS can reassemble to form a rodlike micelle in the ribbon wall and finally to form disordered silica mesostructure with a corresponding increase in the wall thickness and the width of the helical mesoporous ribbon. The reassembly process of the lipid tape with APES and TEOS with maintainance of the ribbon morphology occurred only at temperatures below 0 °C.

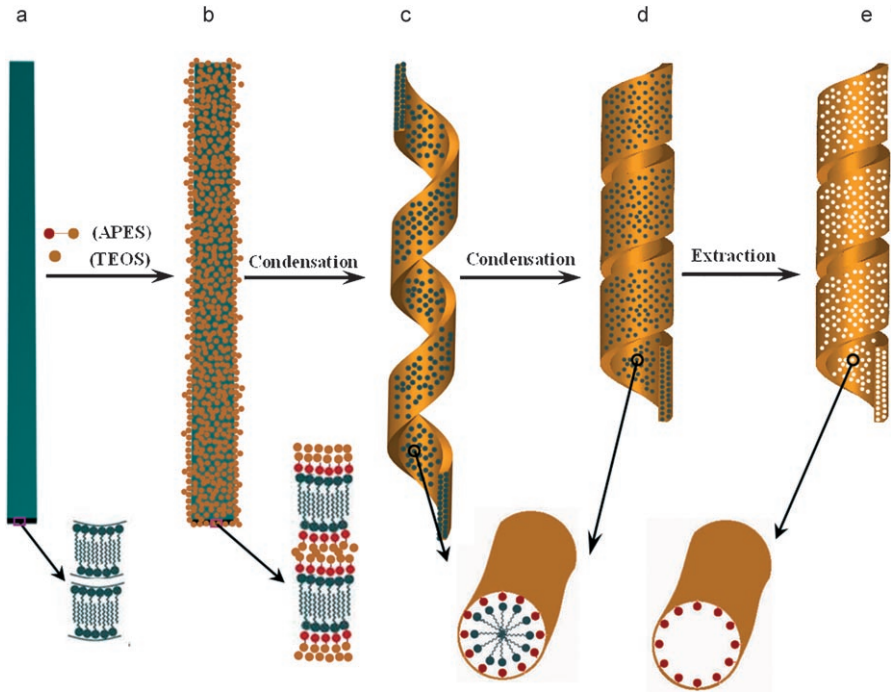

Figure 7. Schematic illustration of the mesoporous silica tape and helical ribbon formation processes.

 © 2008 Wiley-VCH Verlag GmbH & Co. KGaA, Weinheim

Figure 5 and Figure 6 show SEM images and XRD patterns obtained for the composites synthesized at 10, 15, and 20 °C. It can be seen that all of the starting materials are flat tapes and they all show the three peaks indexed as 1, 2, and 3 based on the lamellar symmetry with d_1 spacings of 2.8 nm. The tapes then melted into irregular monoliths with maintainance of the lamellar structures, and then the mixtures comprised particles with two types of dominant morphology, as shown in Figure 5 and Figure 6. One of these has the form of the spheres, disklike structures, and helical hexagonal rods (Figure 5, 10 °C-35 min, 15 °C-30 min, and 20 °C-15 min) that were observed in the final products (Figure 5, 10 °C-2 h, 15 °C-2 h, and 20 °C-25 min), whereas the other exhibited the morphology of the larger irregular monoliths observed in the former samples. The products with hollow spheres with disordered mesostructures and the platelike and helical rods with ordered 2D-hexagonal mesostructures were obtained at synthesis temperatures of 10, 15, and 20 °C, respectively. It can be estimated that, at temperatures higher than 0 °C, the starting-material bilayered tape first melted and then the spherical and rod shapes were created from the melted monoliths through reaction with both APES and TEOS.

The effect of temperature on the formation of the mesostructures can be explained in terms of surfactant packing in this synthetic process. It is known that the packing of the organic surfactant is dominantly effective for the formation of the ordered mesostructures. Surfactants such as amino acid derived amphiphilic lipid molecules self-organize into micelles of various shapes in the equilibrium state. The shape of the micelle has been quantified by the packing parameter, $g = V/a_0 l$, where V is the volume of the hydrophobic chain, a_0 is the effective head-group area per hydrophilic head group, and l is the critical hydrophobic chain length. If $g < 1/3$, the amphiphile has a tendency to form spherical micelles; if $1/3 < g < 1/2$, cylindrical micelles will be favored; if $1/2 < g < 1$, bilayers with spontaneous curvature (vesicles) are produced; if $g = 1$, planar bilayers will be favored.[2] It is known that the packing parameter of the surfactant increases when the temperature decreases, which leads to the formation of aggregates with morphologies including globules, multi- and single-walled vesicles, rods, tubes, and disks with curved and planar bilayers.[11,15] Upon cooling, many types of helical tubes, rods, twisted ribbons, and rolled-up sheets have been obtained in aqueous gels by self-organization of appropriate spherical or sheetlike bilayers made of lipid molecules.[2,16] As the mixture gel is cooled in this synthesis system, the stereorepulsion between the head groups decreases, which leads to a decrease in the effective head-group area and results in an increased g parameter of the micelle; this leads to a transition from cylindrical to bilayered micelles. Therefore, it is reasonable that the HR with a bilayer structure was formed at lower temperatures and other highly ordered mesoporous silicas with curvature were formed at higher temperatures.

Synthesis of mesoporous silica microstructures with antipodal, racemic, and achiral *N*-AAAs: The antipodal amphiphilic molecule *N*-miristoyl-D-alanine (C_{14}-D-Ala) also led to microstructural changes from CMS to a mesoporous HR silica upon cooling of the synthesis system (Figure 8). The

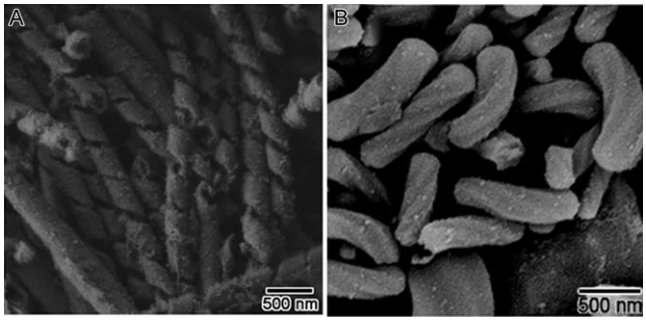

Figure 8. SEM images of extracted mesoporous silicas synthesized with C_{14}-D-AlaA at reaction temperatures of 0 °C (A) and 20 °C (B).

mesoporous silica HR synthesized with C_{14}-L-Ala at 0 °C formed exclusively right-handed HRs, whereas C_{14}-D-Ala gave pure left-handed HRs (Figure 8 A); the CMSs synthesized with C_{14}-L-Ala at 20 °C indicated left-handed excess and with C_{14}-D-Ala indicate right-handed excess (Figure 8 B). These results indicate that the handedness of the mesoporous silica HRs and the CMS was determined by asymmetric structural discrimination in the micelle of the amphiphilic molecule. The left-/right-handed ratio of CMS synthesized with C_{14}-D-Ala has been proved to be 2.5/7.5, which is the opposite of the result in the C_{14}-L-Ala synthesis system.

The racemic molecule (C_{14}-*rac*-Ala) and the achiral *N*-miristoyl glycine (C_{14}-Gly) molecule were not able to produce the HR microstructure (Figure 9 A1 and B1). However, CMS can be formed with both racemic and achiral lipid molecules. It may be assumed from this result that chiral discrimination based on the molecular structure is the dominant factor for the formation of the bilayer lamellar arrangement of the amphiphilic molecules and consequently both the helicity and handedness of the HRs. At lower temperatures, the strong amide hydrogen bonding contributes to the decreased distance between the head groups with chiral carbon atoms, which is favorable for the chiral discrimination and thus results in the enantiopure HRs. The chirality of the asymmetric carbon atoms determines the handedness of the helical structure of the bilayer or the coiled ribbon. On the other hand, ionic and stereorepulsion between the head groups increases with heating, which leads to an increase in the effective head-group area and results in increasing mesophase curvature. The micellar structure of the amphiphiles changed from a frozen bilayer to hollow spheres, disklike, and finally rod-type microstructures with increasing temperature. The larger distance between the head groups is then unfavorable for chiral discrimination of

 © 2008 Wiley-VCH Verlag GmbH & Co. KGaA, Weinheim

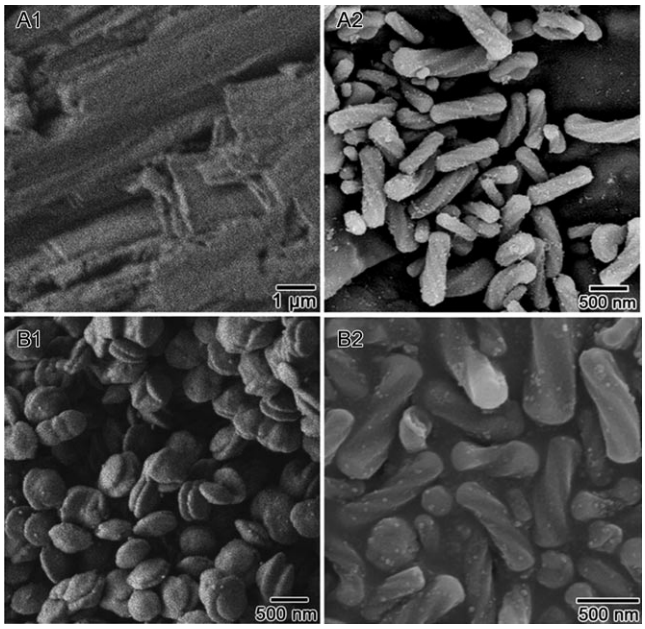

Figure 9. SEM images of extracted mesoporous silicas synthesized with C_{14}-*rac*-AlaA (A) and achiral lipid C_{14}-Gly (B) at reaction temperatures of 0 °C (A1 and B1) and 20 °C (A2 and B2).

the chiral carbon atoms and thus resulted in the formation of enantioimpure 2D-hexagonal mesoporous silica.

The CMS samples synthesized with racemic (C_{14}-*rac*-Ala) and achiral (C_{14}-Gly) lipids at higher temperature were shown to be racemic; that is, the left/right-handed ratios were about 1:1 (Figure 9 A2 and B2). The XRD patterns of all samples synthesized at 0 °C exhibited disordered mesostructures, and all CMS samples synthesized at 20 °C show highly ordered 2D-hexagonal *p6mm* mesostructures, regardless of whether the racemic or achiral lipid molecules were used (results not shown).

^{13}C CP/MAS NMR spectrum of extracted mesoporous silica microstructures: After removal of *N*-AAA, all of these four types of mesoporous silicas can be amino-group-functionalized on the pore surfaces. The absence of surfactant molecules after extraction was proved by ^{13}C CP/MAS NMR spectrum (Figure 10). Almost no resonance signal was detected between $\delta = 20$ and 40 ppm, which would be attributable to the alkyl group of C_{14}-L-AlaS, whereas the resonance signals at $\delta = 10$, 21.7, and 42.6 ppm that are assignable to the C1, C2, and C3 atoms of APES were clearly observed. These spectra demonstrate that the surfactant molecules were almost completely removed, whereas the amine groups remained on the surface of the mesopores. Elemental analysis results showed that the loading amounts of the organic NH_2 groups in samples A–D are all 1.2 mmol per g of SiO_2.

Conclusion

In conclusion, various microstructures that have been observed form lipid-based self-assembly, such as HRs, hollow spheres, disks, and helical rods, have been obtained by variation in the synthesis temperature. The disordered and 2D-hexagonally ordered mesopores in these microstructured silicas have been formed through re-self-assembly of the lipid molecules, CSDA, and silica source. These results demonstrate the effectiveness of the strategy of varying the temperature and using a CSDA with pendant amino groups to initiate silica condensation at the surface of self-organized lipid molecules. It is noteworthy that, at the lowest temperature, the HR was formed through a morphological transition from the flat-tape ribbon, whereas, at higher temperatures, the other microstructures were formed by a melting process with addition of CSDA and TEOS.

To seriously consider the use of molecularly assembled microstructures in a general sense, it is important to understand the relationship between the actual structure of the individual molecules comprising the microstructure and the dimension or geometry of the microstructures. Unfortunately, our understanding has not yet reached this detailed molecular level for the HR formation. HRs and CMS structures with opposite handedness have been synthesized with the same surfactant at different reaction temperatures. Although the formation mechanism of this fascinating structure is still not completely understood, we believe that this will provide a new insight into the molecular factors governing inorganic–organic macro- and mesophase formation and the techno-

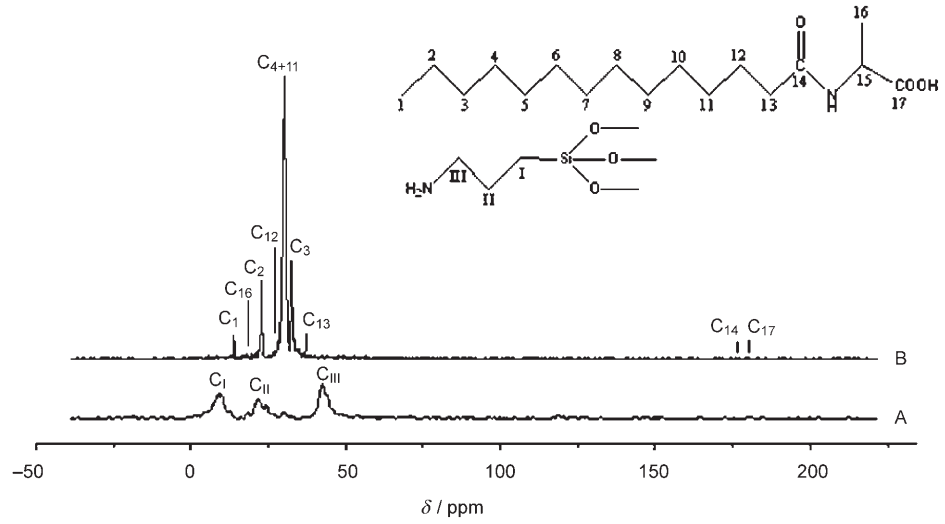

Figure 10. ^{13}C CP/MAS NMR spectra of extracted mesoporous silica HRa (A) and C_{14}-L-AlaS (B).

© 2008 Wiley-VCH Verlag GmbH & Co. KGaA, Weinheim

logical utility of lipid molecules in the most advanced materials applications.

Experimental Section

Materials: C_{14}-L-AlaS, C_{14}-D-Ala, C_{14}-*rac*-Ala, and C_{14}-Gly were synthesized according to previous reports.[17,18] NaOH and HCl were purchased from the Shanghai Chemical Company. TEOS was purchased from TCI and APES (98%) was from Azmax. All chemicals were used as received without further purification.

Synthesis: Different microstructured mesoporous silicas were prepared by using the chiral anionic amphiphilic lipid molecule C_{14}-L-AlaS as a template and APES as a co-structure-directing agent. In a typical synthesis, C_{14}-L-AlaS (0.32 g, 1 mmol) was dissolved in deionized water (17.1 g) with stirring at room temperature. 0.01 M HCl (10 mL) was added to the above solution under vigorous stirring at room temperature to partially neutralize the salt to produce the amino acid. A mixture of TEOS (1.46 g, 7 mmol) and APES (0.22 g, 1 mmol) was then added to the reaction mixture with stirring at 0, 10, 15, or 20 °C. After 10 min of reaction time with stirring, the resultant material was aged at the appropriate temperature for the desired time to get the final product. The products were recovered by centrifugal separation and dried at different temperatures. The lipid molecules were removed by exhaustive solid–liquid extraction overnight by using HCl (1 M) in ethanol or calcination under 550 °C.

Characterization: Powder XRD patterns were recorded on a Rigaku X-ray diffractometer D/MAX-2200/PC equipped with $Cu_{K\alpha}$ radiation (40 kV, 20 mA) at a rate of $0.1°\,min^{-1}$ over the range of 1–6° (2θ). HRTEM was performed with a JEOL JEM-3010 microscope operating at 300 kV (Cs: 0.6 mm; resolution: 1.7 nm). The microscopic features of the sample were observed with SEM by using a JEOL JSM-7401F instrument. The BET surface area and the pore size were obtained from the maxima of the pore-size distribution curve calculated by the Barrett–Joyner–Halenda (BJH) method by using the adsorption branch of the isotherm. The ^{13}C CP/MAS NMR spectrum was measured on a MERCURYplus 400 spectrometer at 100 MHz with a sample spinning frequency of 3 kHz.

Acknowledgements

This work was supported by the National Natural Science Foundation of China (Grant nos.: 20425102 and 20521140450) and the China Ministry of Education. O.T. and Y.S. thank the Swedish Research Council (VR) and the Japan Science and Technology Agency (JST) for financial support and Sam Stevens (Manchester University) for critical reading.

[1] J. M. Schnur, *Science* **1993**, *262*, 1669.
[2] T. Shimizu, M. Masuda, H. Minamikawa, *Chem. Rev.* **2005**, *105*, 1401.
[3] J. H. Jung, S. H. Lee, J. S. Yoo, K. Yoshida, T. Shimizu, S. Shinkai, *Chem. Eur. J.* **2003**, *9*, 5307.
[4] K. Sakata, T. Kunitake, *J. Chem. Soc. Chem. Commun.* **1990**, 504.
[5] a) H. P. Lin, C. Y. Mou, *Science* **1996**, *273*, 765; b) J. H. Jung, Y. Ono, S. Shinkai, *Langmuir* **2000**, *16*, 1643; c) J. H. Jung, S. Shinkai, T. Shimizu, *Chem. Rec.* **2003**, *3*, 212; d) Q. Ji, T. Shimizu, *Chem. Commun.* **2005**, 4411; e) Q. Ji, R. Iwaura, T. Shimizu, *Chem. Mater.* **2007**, *19*, 1329.
[6] a) N. Nakashima, S. Asakuma, T. Kunitake, *J. Am. Chem. Soc.* **1985**, *107*, 509; b) J. H. Jung, H. Kobayashi, M. Masuda, T. Shimizu, S. Shinkai, *J. Am. Chem. Soc.* **2001**, *123*, 8785; c) G. John, J. H. Jung, H. Minamikawa, K. Yoshida, T. Shimizu, *Chem. Eur. J.* **2002**, *8*, 5494; d) J. H. Jung, Y. Do, Y. Lee, T. Shimizu, *Chem. Eur. J.* **2005**, *11*, 5538.
[7] a) J. H. Jung, Y. Ono, S. Shinkai, *Angew. Chem.* **2000**, *112*, 1931; *Angew. Chem. Int. Ed.* **2000**, *39*, 1862; b) Y. Yang, M. Suzuki, S. Owa, H. Shirai, K. Hanabusa, *Chem. Commun.* **2005**, 4462; c) Y. Yang, M. Suzuki, S. Owa, H. Shirai, K. Hanabusa, *J. Mater. Chem.* **2006**, *16*, 1644; d) Y. Yang, M. Suzuki, S. Owa, H. Shirai, *J. Am. Chem. Soc.* **2007**, *129*, 581; e) X. Wu, J. Ruan, T. Ohsuna, O. Terasaki, S. Che, *Chem. Mater.* **2007**, *19*, 1577.
[8] J. H. Jung, Y. Ono, K. Sakurai, M. Sano, S. Shinkai, *J. Am. Chem. Soc.* **2000**, *122*, 8648.
[9] a) S. Che, A. E. Garcia-Bennett, T. Yokoi, K. Sakamoto, H. Kunieda, O. Terasaki, T. Tatsumi, *Nat. Mater.* **2003**, *2*, 801; b) C. Gao, Y. Sakamoto, K. Sakamoto, O. Terasaki, S. Che, *Angew. Chem.* **2006**, *118*, 4401; *Angew. Chem. Int. Ed.* **2006**, *45*, 4295; c) C. Gao, H. Qiu, W. Zeng, Y. Sakamoto, O. Terasaki, K. Sakamoto, Q. Chen, S. Che, *Chem. Mater.* **2006**, *18*, 3904; d) A. E. Garcia-Bennett, O. Terasaki, S. Che, T. Tatsumi, *Chem. Mater.* **2004**, *16*, 813.
[10] S. Che, Z. Liu, T. Ohsuna, K. Sakamto, O. Terasaki, T. Tatsumi, *Nature* **2004**, *429*, 281.
[11] B. N. Thomas, C. R. Safinya, R. J. Plano, N. A. Clark, *Science* **1995**, *267*, 1635.
[12] H. Jin, Z. Liu, T. Ohsuna, O. Terasaki, Y. Inoue, K. Sakamoto, T. Nakanishi, K. Ariga, S. Che, *Adv. Mater.* **2006**, *18*, 593.
[13] I. Toyoko, T. Yoshiyuki, M. Hidetoshi, *J. Am. Chem. Soc.* **1992**, *114*, 3414.
[14] J. M. Schnur, B. R. Ratna, J. V. Selinger, A. Singh, G. Jyothi, K. R. K. Easwaran, *Science* **1994**, *264*, 945.
[15] J. E. Dubois, M. E. Alaoui, J. Toullec, *J. Am. Chem. Soc.* **1981**, *103*, 5401.
[16] J. H. Fuhrhop, C. Boettcher, *J. Am. Chem. Soc.* **1990**, *112*, 1768.
[17] B. G. Trewyn, C. M. Whitman, V. S.-Y. Lin, *Nano Lett.* **2004**, *4*, 2139.
[18] M. Takehara, I. Yoshimura, K. Takizawa, R. Yoshida, *J. Am. Oil Chem. Soc.* **1972**, *49*, 157.

Received: December 18, 2007
Revised: April 3, 2008
Published online: June 9, 2008

 © 2008 Wiley-VCH Verlag GmbH & Co. KGaA, Weinheim